A novel role for fatty acid transport protein 1 in the regulation of tricarboxylic acid cycle and mitochondrial function in 3T3-L1 adipocytes

Brian M. Wiczer and David A. Bernlohr[1]

Department of Biochemistry, Molecular Biology, and Biophysics, University of Minnesota, Minneapolis, MN

Abstract **Fatty acid transport proteins (FATPs) are integral membrane acyl-CoA synthetases implicated in adipocyte fatty acid influx and esterification. Whereas some FATP1 translocates to the plasma membrane in response to insulin, the majority of FATP1 remains within intracellular structures and bioinformatic and immunofluorescence analysis of FATP1 suggests the protein primarily resides in the mitochondrion. To evaluate potential roles for FATP1 in mitochondrial metabolism, we used a proteomic approach following immunoprecipitation of endogenous FATP1 from 3T3-L1 adipocytes and identified mitochondrial 2-oxoglutarate dehydrogenase. To assess the functional consequence of the interaction, purified FATP1 was reconstituted into phospholipid-containing vesicles and its effect on 2-oxoglutarate dehydrogenase activity evaluated. FATP1 enhanced the activity of 2-oxoglutarate dehydrogenase independently of its acyl-CoA synthetase activity whereas silencing of FATP1 in 3T3-L1 adipocytes resulted in decreased activity of 2-oxoglutarate dehydrogenase. FATP1 silenced 3T3-L1 adipocytes exhibited decreased tricarboxylic acid cycle activity, increased cellular NAD^+/NADH, increased fatty acid oxidation, and increased lactate production indicative of altered mitochondrial energy metabolism. These results reveal a novel role for FATP1 as a regulator of tricarboxylic acid cycle activity and mitochondrial function.**—Wiczer, B. M. and D. A. Bernlohr. **A novel role for fatty acid transport protein 1 in the regulation of tricarboxylic acid cycle and mitochondrial function in 3T3-L1 adipocytes.** ***J. Lipid Res.*** **2009.** 50: **2502–2513.**

Supplementary key words fatty acid transport proteins • mitochondria • reconstitution • oxidation • proteomics • alpha-ketoglutarate dehydrogenase • redox homeostasis

Long-chain fatty acid (LCFA) flux in tissues such as cardiac and skeletal muscle, liver, and adipose is a highly regulated and complex process involving both diffusional and protein-mediated components (1–3). A number of proteins have been identified and shown to play roles in LCFA influx (2, 4–7), including fatty acid translocase/CD36, plasma membrane fatty acid-binding protein, caveolin-1, as well as fatty acid transport proteins (FATPs). Members of the FATP family are integral membrane proteins and exhibit CoA- and ATP-dependent long-chain and very long-chain fatty acyl-CoA synthetase activity (8–12). FATPs facilitate LCFA influx at least in part by coupling the diffusion of LCFA through the plasma membrane with CoA-esterification on the inner leaflet of the membrane in a process termed vectoral acylation (13–15).

Mammals possess six FATP isoforms (FATP1–6) that have varying tissue expression and subcellular localization (3, 16, 17). Overexpression of FATPs in mammalian cells results in increased LCFA influx (9, 18–21) and several isoforms, though not all, can rescue the decrease in LCFA influx in yeast lacking the FATP homolog, Fat1p (11). In contrast, functional studies using primary adipocytes and skeletal muscle from FATP1 null mice (22) or FATP1 knockdown 3T3-L1 adipocytes (3) have shown that FATP1 has only a minor role in basal LCFA influx (3, 5). Rather, consistent with the insulin-stimulated translocation of FATP1 to the plasma membrane (5), FATP1 is required for insulin-stimulated LCFA uptake (3, 5). Functional studies of FATP4 have shown that the protein does not play a role in LCFA uptake in either enterocytes (23) or adipocytes (3) but in fat cells may function in fatty acid reesterification following lipolysis (3).

Interestingly, the majority of FATP1 remains on intracellular structures even under insulin-stimulated conditions (3, 5), leading to the possibility of additional roles for FATP1. In this report, we used a proteomic approach to

Supported by 7-06-RA-12 from the American Diabetes Association to D.A.B.

Manuscript received 1 May 2009 and in revised form 16 June 2009.

Published, JLR Papers in Press, June 17, 2009
DOI 10.1194/jlr.M900218-JLR200

Abbreviations: ASM, acid soluble metabolites; DDM, *n*-dodecyl-β-D-maltoside; DOPC, dioleoylphosphatidylcholine; DOPE, dioleoylphosphatidylethanolamine; DOPS, dioleoylphosphatidyl-L-serine; FATP, fatty acid transport protein; LCFA, long-chain fatty acid; OGDH, 2-oxoglutarate dehydrogenase complex; PDH, pyruvate dehydrogenase, shRNA, short hairpin RNA; SUV, small unilamellar vesicle.

[1]To whom correspondence should be addressed.
e-mail: bernl001@umn.edu

identify novel FATP1-interacting proteins in 3T3-L1 adipocytes and identified mitochondrial 2-oxoglutarate dehydrogenase (OGDH), a kinetically rate-limiting step in the tricarboxylic acid cycle, as a binding partner. Using a reconstituted FATP1 proteoliposome system, we find that FATP1 enhances the activity of OGDH in vitro that is independent of FATP1 acyl-CoA synthetase activity. Consistent with this, OGDH activity is decreased in 3T3-L1 adipocytes stably expressing short hairpin (sh)RNA directed at FATP1. These observations are coincident with altered mitochondrial tricarboxylic acid cycle metabolism in the FATP1 knockdown adipocytes, indicating that FATP1 is a novel regulator of mitochondrial function.

MATERIALS AND METHODS

Reagents and cell culture

Cell culture reagents were obtained from Invitrogen. Cell culture-grade porcine insulin, puromycin, methylisobutylxanthine, and dexamethasone were obtained from Sigma-Aldrich. Nonradiolabeled fatty acids were obtained from Nu-Chek Prep, Inc. (Elsyian, MN). [^{3}H]lignoceric acid was obtained from American Radiochemicals Co. [9,10-^{3}H] and [1-^{14}C]palmitate and [2-^{14}C] pyruvate w*ere* obtained from GE Healthcare Life Sciences. *n*-dodecyl-*β*-D-maltoside was obtained from MBL International Corp. Dioleoylphosphatidylcholine (DOPC), dioleoylphosphatidylethanolamine (DOPE), dioleoylphosphatidyl-L-serine (DOPS), and cholesterol were obtained from Avanti Polar Lipids, Inc. Alexa Fluor 488-conjugated goat anti-rabbit IgG was obtained from Invitrogen and IRDye 700-conjugated goat anti-rabbit IgG was obtained from Li-Cor Biosciences. All other reagents were of analytical grade and obtained from Sigma-Aldrich. Differentiation and maintenance of 3T3-L1 cell lines expressing either a shRNA targeting FATP1 or a scrambled sequence was previously described (3).

3T3-L1 adipocyte cross-linking, immunoprecipitation, and proteomic analysis

Formaldehyde cross-linking was performed as described (24), with modifications. Briefly, day 8 3T3-L1 adipocytes were cross-linked with 0.5% formaldehyde for 10 min at room temperature and quenched with 1.5-fold molar excess Tris-HCL pH 7.5. Monolayers were lysed into RIPA buffer (50 mM Tris, pH 7.5, 100 mM NaCl, 50 mM sodium fluoride, 5 mM sodium pyrophosphate, 1% Triton X-100, 1% sodium deoxycholate, 0.1% SDS) containing protease and phosphatase inhibitors, sonicated and centrifuged at 13,000 *g* for 10 min at 4°C to prepare a detergent soluble extract. FATP1 was immunoprecipitated overnight at 4°C using rabbit anti-FATP1 with rabbit preimmune IgG used as a negative control at the same concentration; 20 μg/ml. Immune complex was incubated with protein A-agarose beads for 1 h and washed in RIPA buffer. The immune complex beads were transferred to new tubes and boiled in SDS-loading buffer for 20 min to reverse the cross-linking. The supernatant was subjected to SDS-PAGE and stained for total protein using Sypro Ruby gel stain (Millipore).

Proteomic analysis was applied to either isolated gel bands or the entire sample lane. To analyze the sample lane, the gel segments containing the immunoglobulin heavy chain and light chain bands were excised and discarded. The remaining lane fragments were divided into 10 fractions, reduced, and cysteine residues alkylated with iodoacetic acid. Samples were subjected to trypsin digestion for 24 h at 37°C and peptides were extracted from the gel and applied to a C18 Zip-Tip (Millipore), washed and eluted in 80% acetonitrile/0.1% trifluoroacetic acid. Recovered peptides were subjected to μlC-MS/MS analysis on an LTQ-Orbitrap mass spectrometer. MS/MS spectra were searched using SEQUEST (version 27, rev. 12, ThermoFinnigan, San Jose, CA) against a nonredundant mouse proteome sequence database assuming a maximum of two missed tryptic cleavages per peptide and the results were validated and organized using Scaffold (version Scaffold_2_02_00, Proteome Software Inc., Portland, OR). Reported peptide sequence matches met the following criteria: *1*) all peptides were multiply charged, *2*) the parent mass tolerance was 7 ppm, *3*) two tryptic termini per peptide, and *4*) a minimum of two unique peptides per match with a minimum peptide probability of 70% as specified by the Peptide Prophet algorithm (25). Peptide sequence matches were considered positive interactions if enriched a minimum of 60-fold over the negative control based on normalized spectrum counts.

Immunofluorescence and confocal microscopy

Immunofluorescence analysis of 3T3-L1 adipocytes was performed as described (3) with minor modifications. 3T3-L1 adipocytes grown on glass cover slips were incubated with 100 nM Mitotracker Red CMXRos (Invitrogen) for 20 min at 37°C and fixed in prewarmed 3.7% formaldehyde for 15 min at room temperature. Cells were permeabilized with ice-cold 75% methanol in water for 10 min at −20°C, washed in PBS, and treated with Image IT-FX enhancer (Invitrogen) for 30 min at room temperature. The cover slips were washed and incubated in blocking buffer containing 0.3% Triton X-100, then stained with the rabbit anti-FATP1 antibody and Alexa Fluor 488-conjugated goat anti-rabbit IgG sequentially, each diluted in PBS and 0.3% Triton X-100, and incubated for 1 h at room temperature. Nuclei were stained with 0.2 μg/ml DAPI in PBS for 1 min and viewed using an Olympus FluoView FV1000 inverted confocal microscope. The images were acquired and analyzed using FluoView software.

Purification and reconstitution of purified FATP into SUVs

Purification of murine FATP1-Myc/His was performed as previously described (8, 10). Purified FATP1 was buffer exchanged into buffer A [100 mM Tris, pH 7.5, 150 mM NaCl, 20% (v/v) glycerol] using a desalting column (Zeba Desalt Spin Columns, Thermo Scientific). For reconstitution, lipids dissolved in chloroform were mixed, dried under nitrogen, and buffer A was added for 1 h at room temperature. The lipid solution was vortexed briefly and sonicated until the solution changed from milky to clear. The resulting small unilamellar vesicles (SUVs) were stored at 4°C until used. Purified FATP1 was reconstituted into SUVs at a protein-lipid molar ratio of 1:1000. SUVs were detergent destabilized at room temperature via the addition of dodecylmaltoside to a final concentration of 3.8 mM (0.195% w/v) that led to the onset of vesicle solubilization (26). The dodecylmaltoside concentration of purified FATP was adjusted to 0.195%, added to the lipid-detergent solution, and allowed to incubate with gentle stirring for 10 min at 4°C. Excess dodecylmaltoside was removed by adding CALBIOSORB adsorbent resin (Calbiochem) equilibrated in buffer A. The resin was incubated with the protein-lipid-detergent solution at 4°C with gentle stirring and after 90 min, additional resin was added to remove residual detergent. The FATP1 proteoliposomes were kept on ice and used immediately.

To analyze the orientation of reconstituted FATP1, detergent-purified or reconstituted FATP samples were incubated in the presence of trypsin (Promega) (1:50 trypsin:protein) for various lengths of time and the reaction stopped by boiling in the presence of reducing and denaturing SDS-PAGE loading buffer con-

taining 4% SDS for 10 min. The samples were separated via SDS-PAGE using a 5–15% SDS-polyacrylamide gel and analyzed via immunoblot analysis as previously described (3). Purified or reconstituted FATP were assayed for acyl-CoA synthetase activity by the conversion of [^{3}H]palmitic acid or [^{3}H]lignoceric acid to their CoA derivatives by a modified method from Nagamatsu et al. (27) as previously described (3, 10).

In situ and in vitro oxoglutarate dehydrogenase activity assay

In situ oxoglutarate dehydrogenase activity was measured as described (28) with modifications. Briefly, cells were washed in HBSS and the assay was initiated upon addition of OGDH reaction buffer containing 50 mM Tris, pH 7.6, 5 mM $MgCl_2$, 0.3 mM thiamine pyrophosphate, 3 mM α-ketoglutarate, 3 mM NAD, 0.2 mM CoA, 0.1 mM $CaCl_2$, 0.05 mM EDTA, 0.5 μg/ml rotenone, 0.2% Triton X-100, 3.5% polyvinyl alcohol (MW 7,000–10,000), 0.75 mM nitrotetrazolium blue, and 0.05 mM phenazine methosulfate. After 10 min at room temperature, cells were aspirated and washed in HBSS. Cells were incubated in 5% NP-40 in HBSS overnight at 37°C and sonicated to dissolve the formazan product. Samples were centrifuged at 8,000 *g* for 10 min to remove lipid and absorbance was measured at 555 nm.

For the in vitro activity assay, purified OGDH (Sigma) (or purified pyruvate dehydrogenase complex (Sigma)) was buffer exchanged into 20 mM potassium phosphate, pH 7.3, 20% glycerol. Ten mU of dehydrogenase was assayed for 15 min at 37°C in 250 μl of a modified reaction buffer containing 50 μM fatty acid-free BSA, 50 mM Tris, pH 7.6, 5 mM $MgCl_2$, 0.3 mM thiamine pyrophosphate, 3 mM α-ketoglutarate or 3 mM pyruvate, 3 mM NAD, 0.2 mM CoA, 0.1 mM $CaCl_2$, 0.05 mM EDTA, 5 mM potassium phoshphate, 0.75 mM nitrotetrazolium blue, and 0.05 mM phenazine methosulfate. The reaction was placed on ice for 5 min and centrifuged at 16,000 *g* for 30 min at 4°C. The formazan pellet was dissolved by sonication and the absorbance at 555 nm measured.

Analysis of cellular and mitochondrial fatty acid oxidation

Cellular fatty acid oxidation was performed as described (29). Briefly, 3T3-L1 adipocytes were incubated in growth medium containing 50 μM L-carnitine overnight and serum-starved for 1 h in Krebs-Ringer's HEPES containing 5.4 mM glucose, 1 mM L-carnitine, and 0.1% fatty acid-free BSA. Palmitate oxidation was initiated upon addition of 400 μM [1-^{14}C]palmitate (2 μCi/μmol palmitate) buffered with fatty acid-free BSA (4:1 fatty acid-BSA) and incubated for 1 h at 37°C and 5% CO_2. Media and cells were transferred to glass vials and acidified with 70% perchloric acid. Volatilized $^{14}CO_2$ was absorbed in 1 M NaOH and transferred to liquid scintillation vials for counting. The remaining acidified sample was centrifuged at 2,000 *g* at 4°C and the radioactivity in the supernatant (acid soluble metabolites) determined by liquid scintillation counting.

For mitochondrial fatty acid oxidation, mitochondria were isolated as described (30). A total of 100 μl isolated mitochondria were added to 1 ml fatty acid oxidation buffer (150 μM [1-^{14}C] palmitate (4 μCi/μmole palmitate), 20 mM Tris, pH 7.4, 100 mM sucrose, 10 mM potassium phosphate, 100 mM KCl, 1 mM $MgCl_2$, 1 mM L-carnitine, 0.1 mM malate, 2 mM ATP, 0.1 mM CoA, 1 mM DTT, and 0.3% fatty acid-free BSA) and incubated for 30 min at 37°C. Reactions were acidified to terminate the reaction and the released $^{14}CO_2$ and ^{14}C-acid soluble metabolites determined by scintillation counting.

Analysis of mitochondrial pyruvate oxidation

Pyruvate oxidation was performed as described (31) with modifications. 3T3-L1 adipocytes were incubated in growth medium containing 50 μM L-carnitine overnight and isolated mitochondria were added to 1 ml pyruvate oxidation buffer (1 mM [2-^{14}C] pyruvate (0.5 μCi/μmole pyruvate), 20 mM Tris, pH 7.4, 100 mM sucrose, 10 mM potassium phosphate, 100 mM KCl, 1 mM $MgCl_2$, 2 mM ADP, 0.1 mM CoA, and 1 mM DTT) and incubated for 30 min at 37°C. Reactions were terminated with injection of 200 μl 9 M sulfuric acid and $^{14}CO_2$ was assessed as described previously.

Metabolite quantitation

To measure lactate production, cells were incubated overnight in low-serum DMEM (high-glucose DMEM, 0.5% FBS, and 50 μM L-carnitine) and the medium was collected for lactate quantitation. To measure levels of cellular NAD^+ and NADH, cells were grown as above under normal serum conditions and washed twice in PBS before nucleotide extraction. Lactate and NAD^+/NADH levels were assessed using their respective kits (BioVision) according to the manufacturer's instructions.

Statistical analysis

The data are represented as the mean ± SD or as the mean ± SEM as indicated. Statistical significance was determined using the two-tail Student's *t*-test and one-way ANOVA where appropriate. $P < 0.05$ was considered to be statistically significant.

RESULTS

Previous studies on FATP1 have focused on its role in mediating long- and very long-chain fatty acid influx into adipocytes and muscle cells. As shown originally by Stahl et al. (5) and subsequently by Lobo et al. (3), FATP1 translocates from intracellular sites to the plasma membrane in response to insulin and such translocation mediates, in part, insulin-stimulated fatty acid influx. However, immunolocalization analysis by Lobo et al. indicated that, as opposed to GLUT4 translocation, only a small percentage of FATP1 migrated to the plasma membrane; the vast majority of all FATP1 remained intracellular. Moreover, the appearance of punctate regions of immunofluorescence suggested that FATP1 might be organellar. These observations suggested that FATP1 plays a role independent of mediating plasma membrane fatty acid influx.

Inspection of the FATP1 primary sequence and bioinformatic analysis predicted that the protein is associated with the mitochondrion. To assess this, each of the FATP family members was evaluated using MitoProt II (32) to identify putative mitochondrial targeting sequences and the probability of mitochondrial import (**Table 1**). The analysis predicts with a probability greater than 95% that FATPs 1, 2, and 4 may be imported into the mitochondrion. Work by Stahl et al. (5) has previously shown that FATP1 fractionates with mitochondria and we were able to confirm that observation through a combination of differential centrifugation and immunoblotting (results not shown). As an independent method to demonstrate FATP1 localization with the mitochondrion, immunofluorescence microscopy was used in conjunction with the mitochondrion-specific dye, Mitotracker Red. **Figure 1** shows that FATP1 colocalized with Mitotracker Red and taken together, confirms that FATP1 is in part localized to the adipocyte mitochondrion.

TABLE 1. Probability of murine FATP import into mitochondria

FATP Family Member	Probability of Mitochondrial Import (%)
FATP1	**95.3**
FATP2	**99.6**
FATP3	1.9
FATP4	**97.6**
FATP5	77.7
FATP6	21.9

Peptide sequences of FATP family members were analyzed for mitochondrial targeting sequences and the probability of mitochondrial import was calculated using MitoProt II.

If FATP1 resides in the mitochondrion, it is likely that it functions in conjunction with other proteins. To test this hypothesis, we undertook a proteomics approach to identify such FATP1-interacting partners. To that end, endogenous FATP1 was immunoprecipitated from detergent-solubilized 3T3-L1 adipocytes and subjected the immune complex and associated polypeptides to SDS-PAGE (**Fig. 2**) and Sypro Ruby staining. A protein at ~100 kDa that was routinely observed in multiple experiments but not present in control immunoprecipitates was excised from the gel, trypsin digested, and the resultant peptides analyzed via μLC-MS/MS. The peptides identified matched the E1 subunit of mitochondrial OGDH, a rate-limiting step in the tricarboxylic acid cycle (Fig. 2, **Table 2**). A 90 kDa band was also observed and processed in parallel; however, its identity was not determined.

Because the association between FATP1 and OGDH could have formed following detergent extraction, we used formaldehyde cross-linking as an additional method to evaluate FATP1-OGDH interaction. Mild formaldehyde cross-linking of cells has been used previously to stabilize protein-protein interactions while minimizing nonspecific interactions (33). In this analysis, proteins that directly associate with FATP1 plus secondary interactions between other associated proteins are revealed through the cross-linking. Experimentally, 3T3-L1 adipocyte proteins were cross-linked with formaldehyde, immunoprecipitated with anti-FATP1 antibodies, heated to reverse the cross-links, and the resultant proteins resolved by SDS-PAGE. The regions corresponding to the heavy and light chains were discarded and the remaining segment of the gel divided into 10 sections. Protein in each segment was digested with trypsin and the peptides recovered and analyzed via μLC-MS/MS sequencing. The resulting matches included the target protein FATP1 and OGDH (i.e., the E1, E2, and E3 subunits) (**Table 3**) as well as proteins involved in fatty acid synthesis and oxidation, glucose metabolism, tricarboxylic acid cycle, and branched-chain amino acid metabolism. The level of each protein determined from the FATP1 immunoprecipitation was estimated to be at least 60-fold greater than in the control immunoprecipitates based on normalized spectral counts.

To address the association between FATP1 and OGDH directly, we evaluated the effects of FATP1 on the activity of purified OGDH. We previously reported that the activity of purified FATP1 in DDM-micelles is unstable at 37°C and is rapidly lost within minutes although being stable for several hours at 4°C (10). Because many integral membrane proteins are unstable unless reconstituted into lipid bilayers, we produced FATP1-containing proteoliposomes and evaluated the effects of reconstitution on FATP1 activity. FATP1 was reconstituted using glycerophospholipids that contained oleoyl side chains at the *sn*-1 and *sn*-2 positions because these phospholipids exhibit gel-to-liquid crystal transition temperatures below 4°C, keeping the lipid bilayer fluid during the reconstitution. Preformed SUVs were detergent-destabilized prior to the addition of purified protein and were successfully reconstituted into mixed DOPC-DOPE (3:1) vesicles based on the migration of FATP1 in a 15–60% sucrose gradient (results not shown).

FATP1 is predicted to have a single transmembrane domain separating a 4–10 amino acid N-terminal domain from the catalytic region (34). This suggested that limited tryptic proteolysis could be used to determine the fraction of FATP1 orientated toward the outside of the vesicle versus that orientated inside of the vesicle. Using trypsin sensitivity and an antibody directed toward the catalytic region (amino acids 192–215), FATP1 in DDM-micelles was rapidly proteolyzed producing an immunoreactive stable core peptide of 25 kDa (**Fig. 3A**). Reconstituted FATP1 was also rapidly and completely proteolyzed, generating an immunoreactive stable core peptide of 15 kDa. These results suggested that FATP1 was orientated essentially unidirectionally in an inside-out manner with the catalytic domain located on the exofacial side of the SUV. This characteristic allowed subsequent assessment of acyl-CoA synthetase activity as previously performed in DDM-micelles. Reconstituted FATP1 exhibited a slightly altered structural conformation resulting in the increased accessibility of at least one trypsin cleavage site as observed by the appearance of a core 15 kDa cleavage product rather than the 25 kDa product found for trypsinized FATP1 in DDM-micelles. To compare the thermostability of reconstituted FATP1 in SUVs to that purified in DDM, the acyl-CoA synthetase activity of FATP1 at 37°C was monitored as a function of time (Fig. 3B). The acyl-CoA synthetase activity of FATP1 in DDM-micelles was lost rapidly with a half-life ($t_{1/2}$) of ~1 min. In contrast, reconstituted FATP1 exhibited increased thermostability at 37°C with a half-life of 30–60 min. The

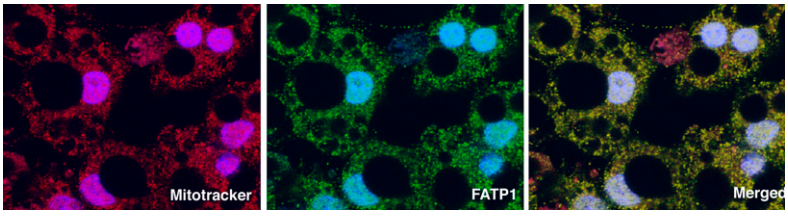

Fig. 1. FATP1 colocalizes with mitochondria in 3T3-L1 adipocytes. 3T3-L1 adipocytes (day 8) were stained with Mitotracker Red and nuclei with DAPI (blue). FATP1 was detected using rabbit anti-FATP1 antibody and Alexa Fluor 488-conjugated goat anti-rabbit IgG (green).

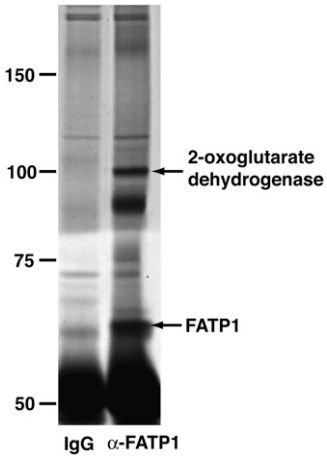

Fig. 2. Immunoprecipitation of FATP1 and association with 2-oxoglutarate dehydrogenase. Control IgG or anti-FATP1 antibody was incubated with detergent-solubilized proteins from 3T3-L1 cells, immunoprecipitated, subjected to SDS-PAGE and stained with Sypro Ruby. The 100 kDa and FATP1 bands were excised and subjected to MS/MS analysis as described in Materials and Methods. Numbers on the left represent M_r in kilodaltons.

activity of reconstituted FATP1 was essentially unaffected by changes in the phospholipid composition or addition of cholesterol (results not shown).

OGDH activity is inhibited in vitro by fatty acyl-CoAs at micromolar levels (35–40). Because of this, we hypothesized that FATP1 would potentially act as an OGDH inhibitor via its acyl-CoA synthetase activity. Having established functional and stable FATP1 proteoliposomes, we assessed the activity of OGDH in the absence or presence of FATP1. Surprisingly, FATP1 enhanced OGDH activity over twofold and was independent of ATP and fatty acids (**Fig. 4A**). Additionally, the increase in OGDH activity was dependent on the concentration of FATP1 (Fig. 4B). Taken together, these results indicate that FATP1 is an OGDH activator independently of acyl-CoA production.

To determine if the ability of FATP1 to enhance OGDH activity occurred in a cellular context, we took advantage of a 3T3-L1 adipocyte cell line stably expressing shRNA directed against FATP1 that we had previously established (**Fig. 5A)** (3) and accessed OGDH activity. Corroborating the in vitro data, OGDH activity was decreased 20% in the FATP1 knockdown adipocytes compared with the scramble shRNA-expressing adipocytes (Fig. 5B). This suggests that FATP1 is a physiological regulator of OGDH.

Because OGDH is a rate-limiting step in the tricarboxylic acid cycle, the decrease in OGDH activity in the FATP1 knockdown adipocytes could also result in decreased tricarboxylic acid cycle activity. To assess this, the rate of [2-^{14}C]pyruvate oxidation was evaluated as a measure of tricarboxylic acid cycle activity (31). As shown in **Fig. 6A**, mitochondria isolated from FATP1 knockdown adipocytes exhibited a 60% reduction in the rate of [2-^{14}C]pyruvate oxidation compared with that in the control mitochondria, indicating a decrease in tricarboxylic acid cycle activity that is consistent with the decrease in OGDH activity.

Because tricarboxylic acid cycle function plays an important role in the cellular redox status, we measured the NAD^+ and NADH levels in the FATP1 knockdown cells. NAD^+ levels were unchanged in the FATP1 silenced adipocytes compared with scramble adipocytes whereas NADH levels were decreased 33% (Fig. 6B, C). There was no sta-

TABLE 2. Identification of ~100 kDa protein coimmunoprecipitated with FATP1 from 3T3-L1 adipocytes

Protein Identified	Accession Number	Mass (kDa)	Seq. Cov.	Peptide Sequence	Xcorr	DCn	-log(e)
oxoglutarate dehydrogenase (E1o subunit)	NP_035086.2	116	19.1%	(K)AEQFYCGDTEGK(K)	0	0	3
				(K)FETPGIMQFTNEEK(R)	0	0	3.85
				(R)FLDTAFDLDAFKK(F)	3.49	0.491	2.64
				(K)ICEEAFTR(S)	2.76	0.238	0
				(R)KPLIVFTPK(S)	2.69	0.201	1.47
				(K)LVEDHLAVQSLIR(A)	4.42	0.492	2.09
				(R)NITLSLVANPSHLEAADPVVMGK(T)	4.51	0.534	6.33
				(R)NMEEEVAITR(I)	3.88	0.296	0
				(K)NQGYYDYVKPR(L)	0	0	2.19
				(R)NTNAGAPPGTAYQSPLSLSR(S)	0	0	5.96
				(R)SSLATMAHAQSLVEAQPNVDK(L)	4.9	0.343	0
				(K)TKAEQFYCGDTEGKK(V)	4.93	0.529	2.72
				(K)VASSVPVENFTIHGGLSR(I)	2.94	0.38	3.2
				(K)VFHLPTTTFIGGQEPALPLR(E)	3.19	0.193	3.3

The 100 kDa band in Fig. 2 was excised and subjected to MS/MS analysis as described in Materials and Methods using the X! Tandem search engine (v2007.01.01.1) in addition. Xcorr and DCn scores generated from SEQUEST and –log(e) scores generated from X! Tandem.

TABLE 3. Identification of proteins coimmunoprecipitated with FATP1 from formaldehyde cross-linked 3T3-L1 adipocytes

Proteins Identified	Accession Number	Mol. Mass	Seq. Cov.	Unique Peptides (#)
Target Protein				
solute carrier family 27, member 1 (FATP1)	NP_036107.1	71 kDa	28.0%	17
Tricarboxylic Acid Cycle				
oxoglutarate dehydrogenase (E1o subunit)	NP_035086.2	116 kDa	50.0%	48
dihydrolipoamide S-succinyltransferase (E2o subunit)	NP_084501.1	49 kDa	41.0%	10
dihydrolipoamide dehydrogenase (E3 subunit)	NP_031887.2	54 kDa	18.0%	7
citrate synthase	NP_080720.1	52 kDa	11.0%	4
isocitrate dehydrogenase 3 (NAD+) α	NP_083849.1	40 kDa	7.9%	3
aconitase 2, mitochondrial	NP_542364.1	85 kDa	2.9%	2
Glycerogenesis and Glycolysis				
aldolase A, fructose-bisphosphate	NP_031464.1	39 kDa	9.3%	3
hexokinase 2	NP_038848.1	103 kDa	3.6%	3
glycerol-3-phosphate dehydrogenase 1 (soluble)	NP_034401.1	38 kDa	8.6%	2
Fatty Acid Metabolism				
acetyl-CoA acyltransferase 1	NP_570934.1	44 kDa	21.0%	8
acetyl-CoA acyltransferase 1B	NP_666342.1	44 kDa	28%	6
ATP citrate lyase	NP_598798.1	120 kDa	5.1%	5
plasma membrane associated protein, S3-12	NP_065593.2	139 kDa	4.2%	5
sterol carrier protein 2, liver	NP_035457.1	59 kDa	7.7%	4
acetyl-CoA acetyltransferase 1 precursor	NP_659033.1	45 kDa	14.0%	4
acyl-CoA dehydrogenase, medium chain	NP_031408.1	46 kDa	11.0%	4
dodecenoyl-CoA delta isomerase	NP_034153.2	32 kDa	19.0%	4
acyl-CoA dehydrogenase, long-chain	NP_031407.2	48 kDa	5.8%	2
acyl-CoA dehydrogenase, short chain	NP_031409.2	45 kDa	6.1%	2
2,4-dienoyl CoA reductase 1, mitochondrial	NP_080448.1	36 kDa	5.1%	2
acyl-CoA synthetase long-chain family member 1	NP_032007.2	78 kDa	3.4%	2
acyl-CoA dehydrogenase family, member 11	NP_780533.2	87 kDa	2.6%	2
carnitine acetyltransferase	NP_031786.2	71 kDa	3.0%	2
Amino Acid Metabolism				
branched chain ketoacid dehydrogenase E1, β	NP_954665.1	36 kDa	14.0%	4
branched chain ketoacid dehydrogenase E1, α	NP_031559.3	51 kDa	9.2%	4
branched chain aminotransferase 2, mitochondrial	NP_033867.1	44 kDa	8.9%	3
glutamate oxaloacetate transaminase 2, mitochondrial	NP_034455.1	47 kDa	8.4%	3
3-hydroxyisobutyrate dehydrogenase precursor	NP_663542.1	35 kDa	9.9%	2
Miscellaneous				
peroxisomal lon protease	NP_080103.1	95 kDa	35.0%	23
oxoglutarate dehydrogenase-like	NP_001074599.1	117 kDa	16.0%	11
unc-84 homolog B	NP_919323.2	78 kDa	13.0%	7
missing oocyte, meiosis regulator, homolog	NP_663349.2	98 kDa	11.0%	7
heat shock protein 1 (chaperonin)	NP_034607.3	61 kDa	5.2%	3
SCY1-like 1	NP_076401.1	89 kDa	3.8%	3
desmoplakin	NP_076331.2	333 kDa	1.0%	3
protein arginine N-methyltransferase 5	NP_038796.2	73 kDa	8.3%	4
adenosine monophosphate deaminase 2 (isoform L)	NP_083055.1	92 kDa	5.8%	4
epoxide hydrolase 2, cytoplasmic	NP_031966.2	63 kDa	12.0%	5
plakophilin 1	NP_062619.1	81 kDa	4.0%	3
nucleoside diphosphate kinase 4	NP_062705.1	21 kDa	31.0%	4
TANK-binding kinase 1	NP_062760.2	83 kDa	8.2%	5
stratifin	NP_061224.2	28 kDa	9.3%	3
heat shock protein 1, β	NP_032328.2	83 kDa	3.6%	2
mitochondrial ribosomal protein S36	NP_079645.1	11 kDa	34.0%	3
glutamyl-prolyl-tRNA synthetase	NP_084011.1	170 kDa	2.1%	2
G protein, β polypeptide 2 like 1	NP_032169.1	35 kDa	8.2%	2
ubiquitin A-52 residue ribosomal protein fusion product 1	NP_001098627.1	15 kDa	23.0%	2
mitochondrial carrier, adenine nucleotide translocator	NP_031476.3	33 kDa	8.4%	2
sec13-like protein isoform a	NP_001034177.1	40 kDa	6.1%	2
actin, γ, cytoplasmic 1	NP_033739.1	42 kDa	10.0%	2
poly(rC) binding protein 1	NP_035995.1	37 kDa	7.0%	2
ATP synthase, mitochondrial F1 complex, γ subunit	NP_001106209.1	30 kDa	7.7%	2
trimethyllysine hydroxylase, epsilon	NP_620097.1	50 kDa	5.5%	2
mitochondrial carrier, citrate transporter	NP_694790.1	34 kDa	5.1%	2

Differentiated 3T3-L1 adipocytes were cross-linked with 0.5% formaldehyde and FATP1 immunoprecipitated. The resultant proteins were separated by SDS-PAGE and subjected to MS/MS analysis as described in Methods and Materials. All identified proteins were enriched at least 60-fold compared with control IgG immunoprecipitate.

tistical change in total NAD levels, however (data not shown). This resulted in a 50% increase in the cellular NAD^+/NADH ratio (Fig. 6D) and is consistent with decreased tricarboxylic acid cycle activity.

The inability to derive energy from mitochondrial metabolism is frequently accompanied by increased metabolism of glucose and fatty acids to compensate for the energy deficiency. This suggests that the FATP1 silenced

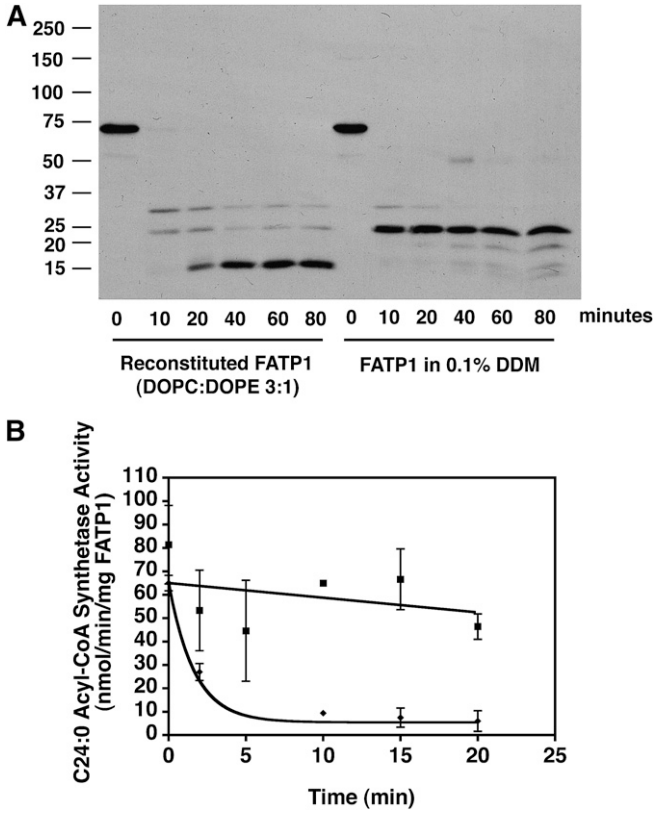

Fig. 3. Reconstitution of FATP1 into small unilamellar vesicles (SUVs) and increased thermostability. A: Reconstituted FATP1 in lipid vesicles comprised of DOPC-DOPE (3:1) or purified FATP1 in DDM-micelles were subjected to trypsin cleavage (1:50 trypsin-protein) for the times indicated, aliquots were removed, added to 4% SDS, subjected to SDS-PAGE and immunoblot analysis using the anti-FATP1 antibody. Numbers on the *y* axis represent M_r in kilodaltons. B: Samples of purified FATP1 in DDM-micelles (♦) or reconstituted FATP1 (■) were incubated at 37°C for 0–20 min. After incubation for the indicated times, the acyl-CoA synthetase activity of the samples was assessed using lignoceric acid (C24:0) as the substrate. Data points are represented as the mean ± SD. The data shown are representative of three independent experiments.

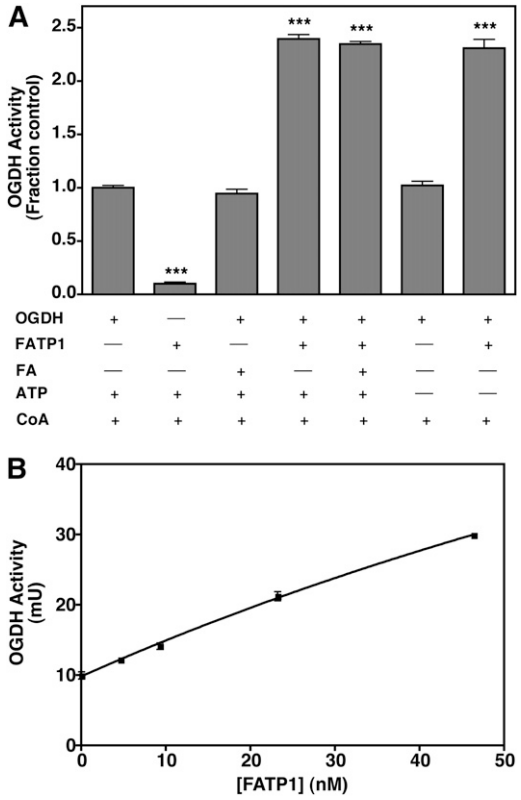

Fig. 4. FATP1 enhances activity of OGDH in vitro. A: The activity of purified OGDH (10 mU) was assessed in the presence or absence of FATP1 proteoliposomes (20 nM FATP1), 250 μM palmitate (FA), or 3 mM ATP. An equivalent amount of lipid vesicles were added when FATP1 was absent; n = 3, mean ± SEM. Statistical analysis using one-way ANOVA with Newman-Keuls posthoc analysis. B: The activity of OGDH was assessed in the absence of ATP and palmitate with increasing concentrations of reconstituted FATP1. Amount of lipid vesicles present was constant; n = 3, mean ± SEM. *** $P < 0.001$ relative to OGDH alone.

adipocytes may exhibit increased glucose metabolism and lactate production. Consistent with this view, lactate production was increased 2.4-fold in the FATP1 knockdown adipocytes (**Fig. 7A**). Similar metabolic changes were seen in cellular fatty acid oxidation where total fatty acid oxidation increased 13% (Fig. 7B). This was due to a 24% increase in the acid soluble metabolites (ASM) produced, whereas complete oxidation of fatty acids (i.e., fatty acids oxidized to CO_2) decreased 30%, consistent with a defect in tricarboxylic acid cycle activity. To eliminate the possibility that the change in fatty acid oxidation is due to other peripheral changes in lipid and glucose metabolism, fatty acid oxidation was measured in isolated mitochondria from the FATP1 silenced cells (Fig. 7C). Similarly, total fatty acid oxidation in isolated mitochondria was increased 17% compared with scramble adipocytes and predominantly due to a 17% increase in ASM. However, unlike what was measured for cellular fatty acid oxidation, complete fatty acid oxidation in isolated mitochondria was increased 11% compared with the scramble adipocytes. This difference may arise from the absence of glucose metabolism in the isolated mitochondria. Consistent with this, the presence of pyruvate attenuates CO_2 production from fatty acids without effecting total fatty acid oxidation (data not shown).

DISCUSSION

FATP1 has been previously demonstrated to play a vital role in insulin-stimulated LCFA influx both in adipocytes (3, 5) and skeletal muscle (5). Consistent with the role of FATP1 in LCFA uptake, FATP1 translocates from intracellular structures to the plasma membrane upon insulin-stimulation; however, a large fraction of FATP1 remains on intracellular structures (3, 5). Several reports have noted the wide subcellular distribution of FATP1 in adipocytes and muscle (3, 5, 41, 42), implying that FATP1 has additional roles in these tissues. Using 3T3-L1 adipocytes as a model system, we took a multidimensional approach to elucidate additional functions of FATP1. Using a combination of immunoprecipitation of endogenous FATP1 and mild formaldehyde cross-linking to stabilize protein-

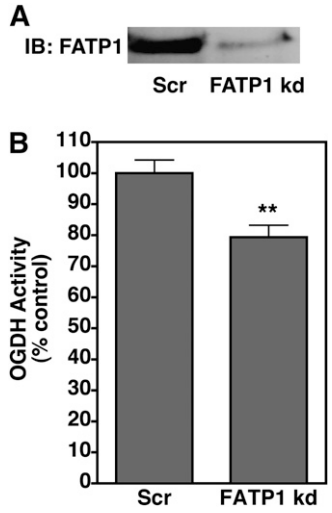

Fig. 5. Analysis of OGDH activity in FATP1 silenced adipocytes. Expression of FATP1 in 3T3-L1 adipocytes stably expressing a scrambled (Scr) or FATP1 shRNA (FATP1 kd) (A) were assayed for OGDH activity for 10 min (B) as described in Materials and Methods; n = 6, mean ± SEM. ** $P < 0.01$ relative to Scr.

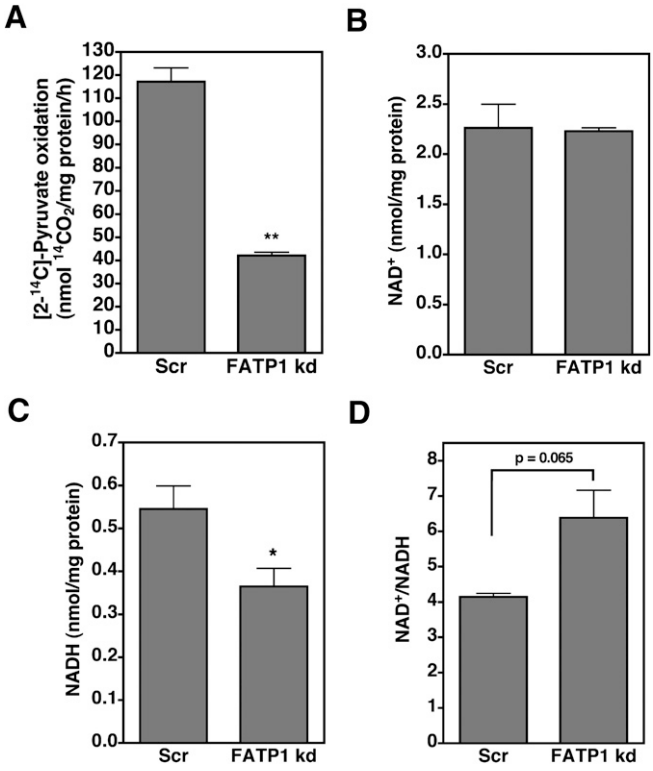

Fig. 6. Tricarboxylic acid cycle activity is decreased in the FATP1 knockdown adipocytes. A: Mitochondria from 3T3-L1 Scr or FATP1 silenced adipocytes pretreated with 50 μM L-carnitine overnight were isolated and incubated with 1 mM [2-^{14}C]pyruvate for 30 min in pyruvate oxidation buffer and $^{14}CO_2$ determined; n = 3, mean ± SEM. B–D: 3T3-L1 Scr or FATP1 knockdown adipocytes were treated similarly and NAD^+ (B), NADH (C), and the NAD^+/NADH ratio determined (D); n = 4, mean ± SEM. * $P < 0.05$; ** $P < 0.01$ relative to Scr.

protein interactions, we identified proteins of the OGDH as a likely binding partner for FATP1. In the absence of cross-linking, the E1 subunit of OGDH was identified as the major FATP1 associated protein (Fig. 2, Table 2). Using cross-linking, a large number of mitochondrial and mitochondrially associated proteins were identified consistent with a large supramolecular complex of multiple proteins and functional activities. Among those identified in the cross-linking experiment was long-chain acyl-CoA synthetase 1 (ACSL1). Richards et al. (15) previously coimmunoprecipitated epitope-tagged FATP1 and ACSL1 using lentiviral overexpression in 3T3-L1 adipocytes. Recent work has shown that ACSL1 is not involved in LCFA influx in adipocytes but may be linked to reesterification of fatty acids following lipolysis (43). Therefore, the true function of the FATP1-ACSL1 interaction is still unknown. These results, in sum, conclude that FATP1 is a mitochondrially-associated protein. Consistent with this, both bioinformatic analysis and immunofluorescence microscopy indicated that FATP1 is localized to mitochondria in 3T3-L1 adipocytes (Table 1, Fig. 1). Moreover, during the preparation of this manuscript, Guitart et al. (44) published work demonstrating that FATP1 localizes to mitochondria in both cultured myotubes and human skeletal muscle. As such, findings in multiple systems conclude that FATP1 has additional functions beyond facilitating fatty acid influx.

To effectively test a functional significance to the proposed FATP1-OGDH interaction, we developed detergent-free FATP1 proteoliposomes for in vitro analysis. FATP1 purified in DDM-micelles is unstable at 37°C (Fig. 3B). However, reconstitution of FATP1 in SUVs resulted in the surprising finding that the enzyme activity was markedly stabilized when maintained at 37°C. Characterization of FATP1 proteoliposomes revealed an approximately 30-fold increase in thermostability compared with FATP1 in DDM-micelles (Fig. 3B). These changes in protein function may be explained by an altered structural conformation in the N-terminal catalytic domain. Consistent with this view, tryptic cleavage of reconstituted FATP1 resulted in a stable 15 kDa protein fragment containing amino acids 192–215 of the N-terminal catalytic domain in contrast to the stable 25 kDa protein fragment generated from FATP1 in DDM-micelles (Fig. 3A). The location of the conformationally sensitive trypsin cleavage site is unknown; however, the $RHRR^{73}$ motif resides adjacent to the predicted amino terminal transmembrane region, suggesting that reconstitution of the protein into SUVs may affect this site, leading to changes in trypsin accessibility. Interestingly, an additional trypsin cleavage site at Lys^{238} resides just C-terminal to the antibody recognition site. This suggests that if the $RHRR^{73}$ motif were inaccessible to trypsin in the DDM-micelles, a 238 amino acid fragment would be produced whereas, in SUVs, a 166 amino acid product would be generated. Because the lipid vesicles represent a more physiological environment and result in increased thermostability of FATP1, the altered structure of FATP1 is believed to represent the natural conformation found in vivo. This suggests that FATP1 proteoliposomes could be used in subsequent in vitro studies.

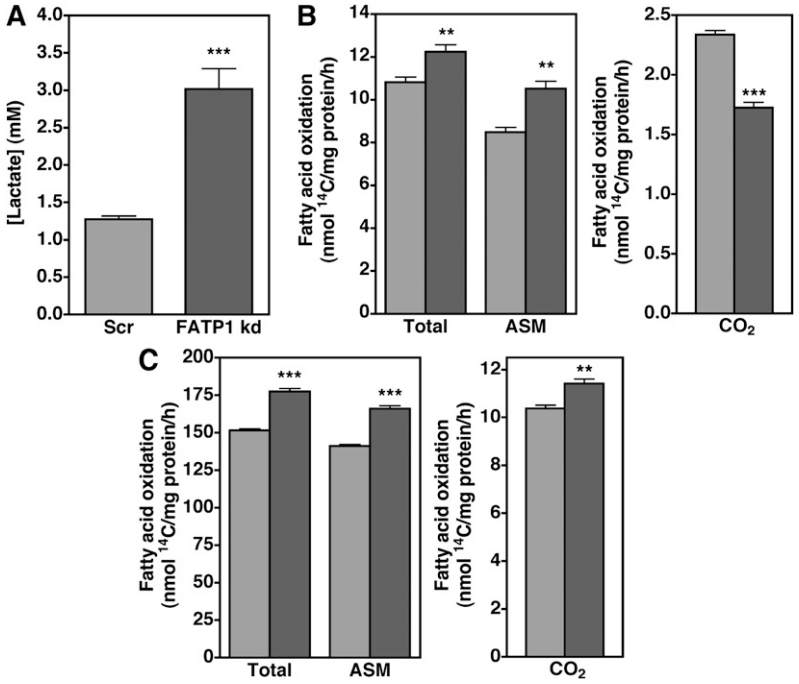

Fig. 7. Lactate production and fatty acid oxidation are increased in the FATP1 silenced adipocytes. A: Lactate in the culture media; n = 6, mean ± SEM. B, C: 3T3-L1 Scr (light gray) or FATP1 knockdown (dark gray) adipocytes were pretreated with 50 μM L-carnitine overnight and fatty acid oxidation assessed in the adipocytes (B) or isolated mitochondria (C) using [1-^{14}C]palmitate. B: n = 6, mean ± SEM. C: n = 4, mean ± SEM. ASM, acid soluble metabolites; Total, ASM + CO_2. ** $P < 0.01$; *** $P < 0.001$ relative to Scr.

Using FATP1 proteoliposomes and purified OGDH, we found that FATP1 enhanced OGDH activity in a concentration-dependent manner that was independent of ATP and fatty acids and, therefore, independent of the acyl-CoA synthetase activity of FATP1 (Fig. 4). This observation was corroborated in the FATP1 knockdown adipocytes where OGDH activity was decreased 20% (Fig. 5). Because we were unable to measure OGDH protein levels due to lack of a functional commercial antibody, we cannot rule out the possibility that OGDH levels are altered in the FATP1 silenced adipocytes. However, because FATP1 was able to enhance purified OGDH activity in vitro, it is strongly suggestive that the interaction is direct and that the loss of FATP1 in the silenced cells is at least in part directly responsible for the observed decrease in the OGDH activity. Fatty acyl-CoAs have been previously shown to attenuate OGDH activity in vitro at low micromolar levels (35–40). Although we were unable to observe any OGDH inhibition in the presence of 6 μM palmitoyl-CoA (data not shown), it is likely that the lipid vesicles in this study act as a sink for fatty acyl-CoAs due to their amphiphilic nature. Therefore, we cannot exclude the possibility that FATP1 acyl-CoA synthetase activity influences OGDH in vivo.

OGDH is one of the rate-limiting steps in the tricarboxylic acid cycle (45, 46) and uses NAD^+ to convert α-ketoglutarate to succinyl-CoA, producing NADH. The NADH produced at this step and subsequent steps in the tricarboxylic acid cycle provide the electrons necessary for maintaining the mitochondrial membrane potential. Because tricarboxylic acid cycle activity is intimately linked to the cellular redox state and energy homeostasis (47–51), we hypothesized that the decrease in OGDH activity in the FATP1 knockdown adipocytes would manifest in decreased tricarboxylic acid cycle activity and further lead to alterations in other energy-producing pathways. We demonstrated that tricarboxylic acid cycle activity is decreased substantially (60%) in the FATP1 knockdown adipocyte mitochondria as measured by [2-^{14}C]pyruvate oxidation (Fig. 6A). This is consistent with the decrease in the NADH levels and, hence, increases in the NAD^+/NADH ratio (Fig. 6C, D), indicating altered mitochondrial energy metabolism. Attenuated tricarboxylic acid cycle activity has also been linked to increases in compensatory glycolysis in the cytoplasm (52–55), in part due to the decrease flux of pyruvate through the tricarboxylic acid cycle as well as increases in fatty acid oxidation (56). Accordingly, lactate production was increased over two-fold (Fig. 7A) and total mitochondrial fatty acid oxidation increased 17% in the FATP1-silenced cells (Fig. 7B, C). Previous work from Lobo et al. (3) has shown that FATP1 knockdown adipocytes have a 10% increase in basal glucose uptake. Although this would in part contribute to an increase in lactate production (57, 58), the magnitude of this increase correlates with the magnitude of the decrease in tricarboxylic acid cycle activity. Further work is needed to explore the mechanistic links between FATP1, tricarboxylic acid activity, and alterations in mitochondrial function.

The work of Guitart et al. (44) also linked FATP1 to glucose oxidation in skeletal myotubes. In their studies, FATP1 overexpression in myotubes resulted in enhanced glucose oxidation whereas fatty acid oxidation was decreased. These results mirror our own observations in the FATP1 knockdown adipocytes. Guitart et al. also found that the increase in glucose oxidation was consistent with an increase in the activity of pyruvate dehydrogenase complex (PDH) although the mechanism through which FATP1 increases the activity of PDH remained unknown. PDH belongs to the 2-oxo acid dehydrogenase superfamily and includes OGDH and the branched-chain keto acid dehydrogenase complex. All three of these dehydrogenase complexes are structurally similar and are comprised of

three subunits (E1, E2, and E3) where the E1 and E2 subunits are unique to each of the dehydrogenases while sharing the same E3 (59). While assessing FATP1 activation of purified OGDH using our FATP1 proteoliposome system, we found that purified PDH was similarly activated by FATP1 in a concentration-dependent manner (data not shown). This suggests that the enhancing ability of FATP1 on OGDH activity also pertains to PDH activity. Furthermore, branched-chain keto acid dehydrogenase was also identified as a candidate FATP1-protein interaction **(Table 3)**. Together, our data suggest the ability of FATP1 to enhance dehydrogenase activity may be conserved for all 2-oxo acid dehydrogenase superfamily members. It is unclear as to why none of the unique PDH subunits were identified as candidate FATP1-protein interactions. One explanation is that the proteins were simply excluded when the IgG gel bands were excised and discarded. Another possibility is that endogenous FATP1 interacts with PDH at relatively low stoichiometry in adipocytes, making it difficult to detect the interaction. Although our current study correlates the decrease in OGDH activity with the decrease in tricarboxylic acid cycle activity in the FATP1 knockdown adipocytes, PDH activity within the knockdowns was not assessed. Therefore, it is possible that a decrease in PDH activity exists in the FATP1 knockdowns and may be contributing to the decreased tricarboxylic acid cycle activity. Further studies are needed to better understand the nature of the physical interactions between FATP1 and the dehydrogenases and the contribution of each of the dehydrogenases to tricarboxylic acid cycle activity in adipocytes.

Interestingly, cardiomyocyte-specific overexpression of FATP1 results in cardiac lipotoxicity (19) whereas *Fatp1*$^{-/-}$ mice maintain insulin sensitivity even on a high-fat diet (7). Although the effects of FATP1 in these systems has been solely considered with regard to fatty acid influx, it is possible that the changes in mitochondrial FATP1 levels and the associated modulation of tricarboxylic acid cycle function also contribute to these phenotypes. *Fatp1*$^{-/-}$ mice are also cold intolerant due to a defect in nonshivering thermogenesis in brown adipose tissue (60). Wu et al. (60) indicated that FATP1 plays an important role in the early phase of thermogenesis as indicated by a decrease in oxygen consumption and CO_2 production prior to the increase in FATP1 protein expression during the late phase of thermogenesis. These observations are also consistent with the decreases in tricarboxylic acid cycle activity and NADH levels we observed in the FATP1 knockdowns and may even result in attenuation of mitochondrial membrane potential in brown adipocytes (61). This would retard the rate of electron transport uncoupling and, in part, attenuate thermogenesis. Additional studies are needed to confirm the role of mitochondrial FATP1 in these systems.

In summary, we demonstrated that FATP1 is localized to mitochondria and enhances OGDH activity in vitro. This is consistent with an attenuation of OGDH activity in cultured FATP1 knockdown adipocytes and correlates with a decrease in tricarboxylic acid cycle activity. Furthermore, the FATP1 knockdown adipocytes have an increased NAD^+/NADH ratio due to decreased NADH levels. These changes in the cellular redox status correlate with the observed increase in lactate production and fatty acid oxidation in the FATP1 knockdowns. This work, along with the work of Guitart et al., reveals a new and novel role for FATP1 in the regulation of tricarboxylic acid cycle function and energy homeostasis via its protein interactions with key proteins in the tricarboxylic acid cycle.

The authors thank Dr. Matthew Stone and the Minnesota Center for Mass Spectrometry and Proteomics for their assistance, the Biomedical Image Processing Lab, the University of Minnesota Supercomputer Institute, and members of the Bernlohr Laboratory for their comments and discussions.

REFERENCES

1. Kampf, J. P., and A. M. Kleinfeld. 2004. Fatty acid transport in adipocytes monitored by imaging intracellular free fatty acid levels. *J. Biol. Chem.* **279:** 35775–35780.
2. Coburn, C. T., F. F. Knapp, Jr., M. Febbraio, A. L. Beets, R. L. Silverstein, and N. A. Abumrad. 2000. Defective uptake and utilization of long chain fatty acids in muscle and adipose tissues of CD36 knockout mice. *J. Biol. Chem.* **275:** 32523–32529.
3. Lobo, S., B. M. Wiczer, A. J. Smith, A. M. Hall, and D. A. Bernlohr. 2007. Fatty acid metabolism in adipocytes: functional analysis of fatty acid transport proteins 1 and 4. *J. Lipid Res.* **48:** 609–620.
4. Zhou, S. L., D. Stump, C. L. Kiang, L. M. Isola, and P. D. Berk. 1995. Mitochondrial aspartate aminotransferase expressed on the surface of 3T3–L1 adipocytes mediates saturable fatty acid uptake. *Proc. Soc. Exp. Biol. Med.* **208:** 263–270.
5. Stahl, A., J. G. Evans, S. Pattel, D. Hirsch, and H. F. Lodish. 2002. Insulin causes fatty acid transport protein translocation and enhanced fatty acid uptake in adipocytes. *Dev. Cell.* **2:** 477–488.
6. Trigatti, B. L., R. G. Anderson, and G. E. Gerber. 1999. Identification of caveolin-1 as a fatty acid binding protein. *Biochem. Biophys. Res. Commun.* **255:** 34–39.
7. Kim, J. K., R. E. Gimeno, T. Higashimori, H. J. Kim, H. Choi, S. Punreddy, R. L. Mozell, G. Tan, A. Stricker-Krongrad, D. J. Hirsch, et al. 2004. Inactivation of fatty acid transport protein 1 prevents fat-induced insulin resistance in skeletal muscle. *J. Clin. Invest.* **113:** 756–763.
8. Hall, A. M., A. J. Smith, and D. A. Bernlohr. 2003. Characterization of the Acyl-CoA synthetase activity of purified murine fatty acid transport protein 1. *J. Biol. Chem.* **278:** 43008–43013.
9. Gimeno, R. E., A. M. Ortegon, S. Patel, S. Punreddy, P. Ge, Y. Sun, H. F. Lodish, and A. Stahl. 2003. Characterization of a heart-specific fatty acid transport protein. *J. Biol. Chem.* **278:** 16039–16044.
10. Hall, A. M., B. M. Wiczer, T. Herrmann, W. Stremmel, and D. A. Bernlohr. 2005. Enzymatic properties of purified murine fatty acid transport protein 4 and analysis of acyl-CoA synthetase activities in tissues from FATP4 null mice. *J. Biol. Chem.* **280:** 11948–11954.
11. DiRusso, C. C., H. Li, D. Darwis, P. A. Watkins, J. Berger, and P. N. Black. 2005. Comparative biochemical studies of the murine fatty acid transport proteins (FATP) expressed in yeast. *J. Biol. Chem.* **280:** 16829–16837.
12. DiRusso, C. C., D. Darwis, T. Obermeyer, and P. N. Black. 2008. Functional domains of the fatty acid transport proteins: studies using protein chimeras. *Biochim. Biophys. Acta.* **1781:** 135–143.
13. Zou, Z., F. Tong, N. J. Faergeman, C. Borsting, P. N. Black, and C. C. DiRusso. 2003. Vectorial acylation in Saccharomyces cerevisiae. Fat1p and fatty acyl-CoA synthetase are interacting components of a fatty acid import complex. *J. Biol. Chem.* **278:** 16414–16422.
14. Tong, F., P. N. Black, R. A. Coleman, and C. C. DiRusso. 2006. Fatty acid transport by vectorial acylation in mammals: roles played by different isoforms of rat long-chain acyl-CoA synthetases. *Arch. Biochem. Biophys.* **447:** 46–52.
15. Richards, M. R., J. D. Harp, D. S. Ory, and J. E. Schaffer. 2006. Fatty acid transport protein 1 and long-chain acyl coenzyme A synthetase 1 interact in adipocytes. *J. Lipid Res.* **47:** 665–672.

16. Ortegren, U., L. Yin, A. Ost, H. Karlsson, F. H. Nystrom, and P. Stralfors. 2006. Separation and characterization of caveolae subclasses in the plasma membrane of primary adipocytes; segregation of specific proteins and functions. *FEBS J.* **273:** 3381–3392.
17. Watkins, P. A. 2008. Very-long-chain acyl-CoA synthetases. *J. Biol. Chem.* **283:** 1773–1777.
18. Stahl, A., D. J. Hirsch, R. E. Gimeno, S. Punreddy, P. Ge, N. Watson, S. Patel, M. Kotler, A. Raimondi, L. A. Tartaglia, et al. 1999. Identification of the major intestinal fatty acid transport protein. *Mol. Cell.* **4:** 299–308.
19. Chiu, H. C., A. Kovacs, R. M. Blanton, X. Han, M. Courtois, C. J. Weinheimer, K. A. Yamada, S. Brunet, H. Xu, J. M. Nerbonne, et al. 2005. Transgenic expression of fatty acid transport protein 1 in the heart causes lipotoxic cardiomyopathy. *Circ. Res.* **96:** 225–233.
20. Schaffer, J. E., and H. F. Lodish. 1994. Expression cloning and characterization of a novel adipocyte long chain fatty acid transport protein. *Cell.* **79:** 427–436.
21. Hatch, G. M., A. J. Smith, F. Y. Xu, A. M. Hall, and D. A. Bernlohr. 2002. FATP1 channels exogenous FA into 1,2,3-triacyl-sn-glycerol and down-regulates sphingomyelin and cholesterol metabolism in growing 293 cells. *J. Lipid Res.* **43:** 1380–1389.
22. Wu, Q., A. M. Ortegon, B. Tsang, H. Doege, K. R. Feingold, and A. Stahl. 2006. FATP1 is an insulin-sensitive fatty acid transporter involved in diet-induced obesity. *Mol. Cell. Biol.* **26:** 3455–3467.
23. Shim, J., C. L. Moulson, E. P. Newberry, M. H. Lin, Y. Xie, S. M. Kennedy, J. H. Miner, and N. O. Davidson. 2009. Fatty acid transport protein 4 is dispensable for intestinal lipid absorption in mice. *J. Lipid Res.* **50:** 491–500.
24. Thompson, B. R., A. M. Muzurkiewicz-Muñoz, J. Suttles, C. Carter-Su, and D. A. Bernlohr. 2009. Interaction of adipocyte fatty acid binding protein and JAK2: AFABP/aP2 as a regulator of JAK2 signaling. *J Biol. Chem.* 284: 13473–13480.
25. Keller, A., A. I. Nesvizhskii, E. Kolker, and R. Aebersold. 2002. Empirical statistical model to estimate the accuracy of peptide identifications made by MS/MS and database search. *Anal. Chem.* **74:** 5383–5392.
26. Knol, J., L. Veenhoff, W. J. Liang, P. J. Henderson, G. Leblanc, and B. Poolman. 1996. Unidirectional reconstitution into detergent-destabilized liposomes of the purified lactose transport system of Streptococcus thermophilus. *J. Biol. Chem.* **271:** 15358–15366.
27. Nagamatsu, K., S. Soeda, M. Mori, and Y. Kishimoto. 1985. Lignoceroyl-coenzyme A synthetase from developing rat brain: partial purification, characterization and comparison with palmitoyl-coenzyme A synthetase activity and liver enzyme. *Biochim. Biophys. Acta.* **836:** 80–88.
28. Park, L. C., N. Y. Calingasan, K. F. Sheu, and G. E. Gibson. 2000. Quantitative alpha-ketoglutarate dehydrogenase activity staining in brain sections and in cultured cells. *Anal. Biochem.* **277:** 86–93.
29. Koves, T. R., J. R. Ussher, R. C. Noland, D. Slentz, M. Mosedale, O. Ilkayeva, J. Bain, R. Stevens, J. R. Dyck, C. B. Newgard, et al. 2008. Mitochondrial overload and incomplete fatty acid oxidation contribute to skeletal muscle insulin resistance. *Cell Metab.* **7:** 45–56.
30. Koves, T. R., R. C. Noland, A. L. Bates, S. T. Henes, D. M. Muoio, and R. N. Cortright. 2005. Subsarcolemmal and intermyofibrillar mitochondria play distinct roles in regulating skeletal muscle fatty acid metabolism. *Am. J. Physiol. Cell Physiol.* **288:** C1074–C1082.
31. Willems, H. L., T. F. de Kort, F. J. Trijbels, L. A. Monnens, and J. H. Veerkamp. 1978. Determination of pyruvate oxidation rate and citric acid cycle activity in intact human leukocytes and fibroblasts. *Clin. Chem.* **24:** 200–203.
32. Claros, M. G., and P. Vincens. 1996. Computational method to predict mitochondrially imported proteins and their targeting sequences. *Eur. J. Biochem.* **241:** 779–786.
33. Sutherland, B. W., J. Toews, and J. Kast. 2008. Utility of formaldehyde cross-linking and mass spectrometry in the study of protein-protein interactions. *J. Mass Spectrom.* **43:** 699–715.
34. Lewis, S. E., L. L. Listenberger, D. S. Ory, and J. E. Schaffer. 2001. Membrane topology of the murine fatty acid transport protein 1. *J. Biol. Chem.* **276:** 37042–37050.
35. Bunik, V. I., G. Raddatz, R. J. Wanders, and G. Reiser. 2006. Brain pyruvate and 2-oxoglutarate dehydrogenase complexes are mitochondrial targets of the CoA ester of the Refsum disease marker phytanic acid. *FEBS Lett.* **580:** 3551–3557.
36. Smith, C. M., J. Bryla, and J. R. Williamson. 1974. Regulation of mitochondrial alpha-ketoglutarate metabolism by product inhibition at alpha-ketoglutarate dehydrogenase. *J. Biol. Chem.* **249:** 1497–1505.
37. Garland, P. B. 1964. Some kinetic properties of pig-heart oxoglutarate dehydrogenase that provide a basis for metabolic control of the enzyme activity and also a stoicheiometric assay for coenzyme A in tissue extracts. *Biochem. J.* **92:** 10C–12C.
38. Gomazkova, V. S., and O. E. Krasovskaia. 1979. [Regulation of alpha-ketoglutarate dehydrogenase complex from pigeon breast muscle] *Biokhimiia.* **44:** 1126–1136.
39. Hamada, M., K. Koike, Y. Nakaula, T. Hiraoka, and M. Koike. 1975. A kinetic study of the alpha-keto acid dehydrogenase complexes from pig heart mitochondria. *J. Biochem.* **77:** 1047–1056.
40. Kornfeld, S., M. Benziman, and Y. Milner. 1977. Alpha-ketoglutarate dehydrogenase complex of Acetobacter xylinum. Purification and regulatory properties. *J. Biol. Chem.* **252:** 2940–2947.
41. Gargiulo, C. E., S. M. Stuhlsatz-Krouper, and J. E. Schaffer. 1999. Localization of adipocyte long-chain fatty acyl-CoA synthetase at the plasma membrane. *J. Lipid Res.* **40:** 881–892.
42. Garcia-Martinez, C., M. Marotta, R. Moore-Carrasco, M. Guitart, M. Camps, S. Busquets, E. Montell, and A. M. Gomez-Foix. 2005. Impact on fatty acid metabolism and differential localization of FATP1 and FAT/CD36 proteins delivered in cultured human muscle cells. *Am. J. Physiol. Cell Physiol.* **288:** C1264–C1272.
43. Lobo, S., B. M. Wiczer, and D. A. Bernlohr. 2009. Functional analysis of long-chain acyl-CoA synthetase 1 in 3T3–L1 adipocytes. *J. Biol. Chem.* 284: 18347–18356.
44. Guitart, M., A. L. Andreu, E. Garcia-Arumi, P. Briones, E. Quintana, A. M. Gomez-Foix, and C. Garcia-Martinez. 2009. FATP1 localizes to mitochondria and enhances pyruvate dehydrogenase activity in skeletal myotubes. *Mitochondrion.* 9: 266–272.
45. Huang, H. M., H. Zhang, H. Xu, and G. E. Gibson. 2003. Inhibition of the alpha-ketoglutarate dehydrogenase complex alters mitochondrial function and cellular calcium regulation. *Biochim. Biophys. Acta.* **1637:** 119–126.
46. Naveri, H. K., H. Leinonen, K. Kiilavuori, and M. Harkonen. 1997. Skeletal muscle lactate accumulation and creatine phosphate depletion during heavy exercise in congestive heart failure. Cause of limited exercise capacity? *Eur. Heart J.* **18:** 1937–1945.
47. Pan, Y., K. D. Mansfield, C. C. Bertozzi, V. Rudenko, D. A. Chan, A. J. Giaccia, and M. C. Simon. 2007. Multiple factors affecting cellular redox status and energy metabolism modulate hypoxia-inducible factor prolyl hydroxylase activity in vivo and in vitro. *Mol. Cell. Biol.* **27:** 912–925.
48. Mailloux, R. J., R. Beriault, J. Lemire, R. Singh, D. R. Chenier, R. D. Hamel, and V. D. Appanna. 2007. The tricarboxylic acid cycle, an ancient metabolic network with a novel twist. *PLoS One.* **2:** e690.
49. Fernie, A. R., F. Carrari, and L. J. Sweetlove. 2004. Respiratory metabolism: glycolysis, the TCA cycle and mitochondrial electron transport. *Curr. Opin. Plant Biol.* **7:** 254–261.
50. Hausler, N., J. Browning, M. Merritt, C. Storey, A. Milde, F. M. Jeffrey, A. D. Sherry, C. R. Malloy, and S. C. Burgess. 2006. Effects of insulin and cytosolic redox state on glucose production pathways in the isolated perfused mouse liver measured by integrated 2H and 13C NMR. *Biochem. J.* **394:** 465–473.
51. Wlodek, D., and M. Gonzales. 2003. Decreased energy levels can cause and sustain obesity. *J. Theor. Biol.* **225:** 33–44.
52. Durkot, M. J., L. De Garavilla, D. Caretti, and R. Francesconi. 1995. The effects of dichloroacetate on lactate accumulation and endurance in an exercising rat model. *Int. J. Sports Med.* **16:** 167–171.
53. Dienel, G. A., and L. Hertz. 2001. Glucose and lactate metabolism during brain activation. *J. Neurosci. Res.* **66:** 824–838.
54. Weiss, R. G., V. P. Chacko, J. D. Glickson, and G. Gerstenblith. 1989. Comparative 13C and 31P NMR assessment of altered metabolism during graded reductions in coronary flow in intact rat hearts. *Proc. Natl. Acad. Sci. USA.* **86:** 6426–6430.
55. Southam, A. D., J. M. Easton, G. D. Stentiford, C. Ludwig, T. N. Arvanitis, and M. R. Viant. 2008. Metabolic changes in flatfish hepatic tumours revealed by NMR-based metabolomics and metabolic correlation networks. *J. Proteome Res.* **7:** 5277–5285.
56. Randle, P. J., P. B. Garland, C. N. Hales, and E. A. Newsholme. 1963. The glucose fatty-acid cycle. Its role in insulin sensitivity and the metabolic disturbances of diabetes mellitus. *Lancet.* **1:** 785–789.
57. Gaidhu, M. P., S. Fediuc, and R. B. Ceddia. 2006. 5-Aminoimidazole-4-carboxamide-1-beta-D-ribofuranoside-induced AMP-activated protein kinase phosphorylation inhibits basal and insulin-stimulated glucose uptake, lipid synthesis, and fatty acid oxidation in isolated rat adipocytes. *J. Biol. Chem.* **281:** 25956–25964.

58. Hwang, D. Y., and F. Ismail-Beigi. 2002. Glucose uptake and lactate production in cells exposed to CoCl(2) and in cells overexpressing the Glut-1 glucose transporter. *Arch. Biochem. Biophys.* **399:** 206–211.
59. Bunik, V. I., and D. Degtyarev. 2008. Structure-function relationships in the 2-oxo acid dehydrogenase family: substrate-specific signatures and functional predictions for the 2-oxoglutarate dehydrogenase-like proteins. *Proteins.* **71:** 874–890.
60. Wu, Q., M. Kazantzis, H. Doege, A. M. Ortegon, B. Tsang, A. Falcon, and A. Stahl. 2006. Fatty acid transport protein 1 is required for nonshivering thermogenesis in brown adipose tissue. *Diabetes.* **55:** 3229–3237.
61. Talbot, J., J. N. Barrett, E. F. Barrett, and G. David. 2007. Stimulation-induced changes in NADH fluorescence and mitochondrial membrane potential in lizard motor nerve terminals. *J. Physiol.* **579:** 783–798.